ARTICLE

Stimuli-Responsive Liposome Fusion Mediated by Gold Nanoparticles

Dissaya Pornpattananangkul,[†,‡] Sage Olson,[†,‡] Santosh Aryal,[†,‡] Marta Sartor,[†,‡] Chun-Ming Huang,[‡,§] Kenneth Vecchio,[†] and Liangfang Zhang[†,‡,*]

[†]Department of Nanoengineering, [‡]Moores Cancer Center, and [§]Division of Dermatology, University of California at San Diego, La Jolla, California 92093

ABSTRACT We report a new approach to controlling the fusion activity of liposomes by adsorbing carboxyl-modified gold nanoparticles to the outer surface of phospholipid liposomes. The bound gold nanoparticles can effectively prevent liposomes from fusing with one another at neutral pH value, while at acidic environments (*e.g.*, pH < 5), the gold particle stabilizers will detach from the liposomes, with liposome fusion activity resuming. The binding of carboxyl-modified gold nanoparticles to cationic phospholipid liposomes at neutral pH and detaching at acidic pH values are evaluated and confirmed by dynamic light scattering, electron microscopy, fluorescence and UV−vis absorption experiments. The relative fusion efficiency of gold-nanoparticle-stabilized cationic liposomes with anionic liposomes is ∼25% at pH = 7 in contrast to ∼80% at pH = 4. Since liposomes have been extensively used as drug nanocarriers and the infectious lesions on human skin are typically acidic with a pH < 5, these acid-responsive liposomes with tunable fusion ability hold great promise for dermal drug delivery to treat a variety of skin diseases such as acne vulgaris and staph infections.

KEYWORDS: phospholipid liposome · nanoparticle · vesicle fusion · acid-responsive · drug delivery

Liposomes are spherical lipid vesicles with a bilayered membrane structure consisting of amphiphilic lipid molecules. They have been recognized as one of the most widely used carriers for delivering a myriad of cosmeticeuticals, pharmaceuticals, and diagnostic and imaging agents.[1] Liposomes can carry both hydrophilic and hydrophobic agents with high efficiency and protect them from undesired effects of external conditions. Their surface can be readily functionalized with specific ligands that target liposomes and their payloads to the sites of action. In addition, the composition, size, surface charge, and other formulation properties of liposomes can be well-controlled to meet the needs of specific circumstances.[1−4] However, the applications of liposomes are usually limited by their instability. Liposomes, particularly with sub-100 nm size, are prone to fuse with one another to reduce their surface tension, leading to payload loss or undesired mixing.[5−8] Moreover, the resulting liposomes with a size much larger than 100 nm are unlikely to transport through the skin, therefore significantly diminishing their use as a dermal drug delivery vehicle.[9,10]

A few strategies have been employed to overcome this problem aiming at improving the use of liposomes as a potent delivery nanocarrier.[11−14] One extensively used approach is to coat the liposome surface with a "stealth" material such as polyethylene glycol (PEG).[15,16] The PEG layer not only prevents liposomes from fusing with one another but also enhances their *in vivo* circulation lifetime by suppressing plasma proteins from adsorbing onto the liposome surface. The success of PEGylated liposomes has led to a group of clinically approved therapeutic products for systemic drug delivery, including Doxil, AmBisome, DaunoXome, DepoCyt, and Visudyne.[3,17] Although the polymer-coated liposomes have shown great success for systemic drug delivery, they are less frequently used for dermal drug delivery, especially to treat bacterial infections. This is because the polymer coating will not only stabilize liposomes against fusion with one another but also prevent them from fusing with bacterial membranes, to which the antimicrobial payloads will be delivered. It is worth noting that bacteria usually interact with vesicular drug nanocarriers such as liposomes in a different manner from host cells or cancerous cells. The cells can internalize the entire liposomes through endocytosis, while the bacteria preferentially go through membrane−membrane fusion.[10,18] Therefore, it would be desirable to develop liposomes that are stabilized against fusion with one another before they are placed at the sites of action including the manufacturing and storage periods, while their

*Address correspondence to zhang@ucsd.edu.

Received for review December 20, 2009 and accepted March 08, 2010.

Published online March 17, 2010.
10.1021/nn9018587

© 2010 American Chemical Society

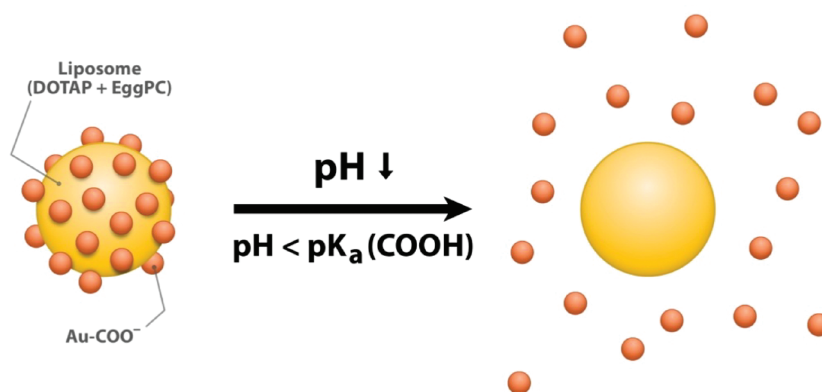

Figure 1. Schematic illustrations of carboxyl-modified gold nanoparticle (AuC)-stabilized liposome and its destabilization at acidic pH. The liposome is stabilized by deprotonated AuC ($Au-COO^-$) at neutral pH. When pH drops below the pK_a value of the carboxylic group (pK_a ~ 5), $Au-COO^-$ nanoparticles are protonated to form Au−COOH, which subsequently detach from the liposome, resulting in the formation of a bare liposome with fusion activity resuming.

fusion activity will be reinstalled once they are applied onto the target skin sites.

Here we report a stimuli-responsive novel gold-nanoparticle-stabilized liposome system in which small gold nanoparticles (diameter ~4 nm) bind to the surface of liposomes (diameter = sub-100 nm) and thus stabilize the liposomes at neutral pH. The bound gold particle stabilizers detach from the liposomes when the environment acidity increases to pH < 5, resulting in the formation of bare liposomes that can actively fuse with various biological membranes. It has been well-documented that human skin is typically acidic (pH = 3.9−6.0),[19] especially the infectious lesions on the skin.[20] For example, the pH value is about 4.0 at the acne lesions[21] and 4.5−6.3 at comedones.[22] Therefore acid-responsive liposomes with tunable fusion ability will be practically demanded for dermal drug delivery. Recently, Granick *et al.* have reported that binding small polystyrene particles (diameter ~20 nm) to the surface of zwitterionic liposomes (diameter ~200 nm) can stabilize liposomes against fusion.[8,23,24] However, no study, to the best of our knowledge, has been reported to develop stimuli-responsive nanoparticle-stabilized liposomes for possible drug delivery applications.

The principle of this study, applying carboxyl-modified gold nanoparticles to mediate the fusion activity of phospholipid liposomes, is illustrated in Figure 1. With a p$K_a \approx 5$,[25] the carboxylic group is deprotonated at pH = 7, resulting in negatively charged $Au-COO^-$ nanoparticles, which can bind to cationic liposomes through electrostatic attraction and thus stabilize the liposomes. When the environment pH drops to below 5, the carboxylic group will be protonated. The resulting neutral Au−COOH nanoparticles will detach from the liposome surface due to the lacking of binding forces, thereby freeing the liposomes. Gold nanoparticles are selected for this study because of their fluorescence quenching properties that can be employed to indicate their binding and detaching process and extent when a small fraction of fluorescent dyes is doped into the liposome membranes. Moreover, gold is a biocompatible noble metal[26] with antimicrobial activity against a wide variety of bacteria.[27]

RESULTS AND DISCUSSION

We first prepared carboxyl-modified gold nanoparticle (AuC)-stabilized liposomes (AuC-liposome). In the study, cationic phospholipid liposomes consisting of 90 wt % hydrogenated L-α-phosphatidylcholine (EggPC) and 10 wt % 1,2-di-(9*Z*-octadecenoyl)-3-trimethylammonium propane (DOTAP) were prepared through the well-known extrusion method.[28] Dynamic

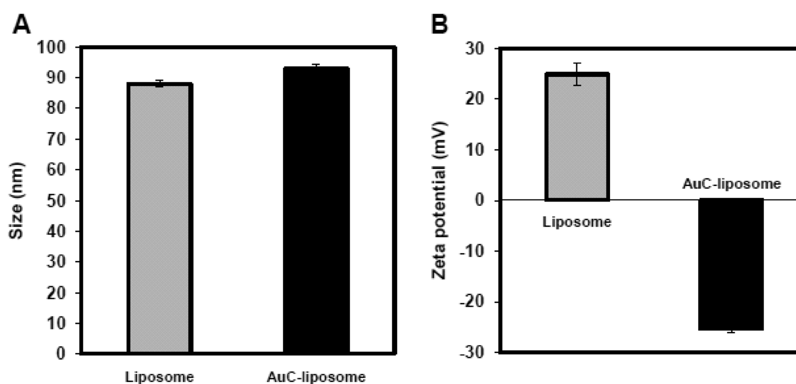

Figure 2. Characterization of AuC-liposome by dynamical light scattering. (A) Size (diameter, nm) and (B) surface ζ potential (mV) of bare liposomes and AuC-liposome with a AuC/liposome molar ratio of 200/1.

light scattering (DLS) measurements showed that the size and surface ζ potential of the formed liposomes were 88.0 ± 1.0 nm and 24.9 ± 2.3 mV, respectively (Figure 2). The positive ζ potential value indicates the incorporation of DOTAP to the liposome membrane. In a separate reaction, AuC nanoparticles were synthesized following a previously published protocol,[29,30] resulting in AuC with a nearly uniform size of ~4 nm measured by scanning transmission electron microscope (STEM) (Figure 3) and a negative surface ζ potential of −25.6 ± 4.2 mV determined by DLS. The synthesized cationic liposomes and AuC nanoparticles were then mixed with a molar ratio of 1:200 under gentle bath sonication for 10 min to form AuC-liposome. The excess AuC in the solution was removed by 10 min centrifugation at 1.3×10^4 rpm to ensure the subsequent particle size and surface ζ potential measurements were solely from the AuC-liposome but not from unbound AuC particles. DLS data showed that the size of the AuC-liposome was 92.9 ± 1.3 nm and the surface ζ potential was −25.3 ± 0.7 mV (Figure 2). The measured AuC-liposome size was slightly larger than that of bare liposomes because of the adsorption of 4 nm AuC nanoparticles, while the change of ζ potential from 24.9 to −25.3 mV explicitly suggests the binding of negatively charged AuC to the positively charged liposomes. The morphology and structure of the AuC-liposome were further imaged by STEM. As shown in Figure 3A,B, individual AuC particles were visible on the surface of liposomes after they were deposited on a TEM grid. Using the energy-dispersive X-ray (EDX) spectrometer on the STEM, we were able to identify elementally that certain regions in Figure 3A,B contained Au and other regions contained only elements found in the liposome, such as carbon and phosphorus. The size of dehydrated liposomes was larger than the size of hydrated liposomes measured by DLS due to the collapse of liposomes from a three-dimensional sphere to a two-dimensional thin layer.

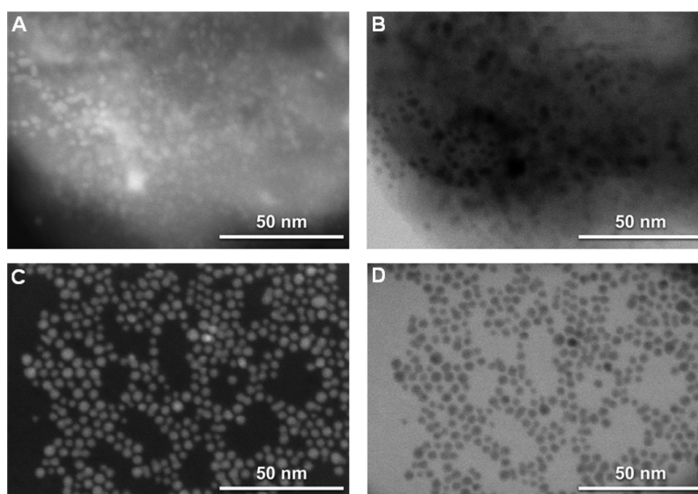

Figure 3. Representative scanning transmission electron microscope (STEM) images showing the structure of AuC-liposome. (A) Secondary electron image shows that AuC nanoparticles adsorb on the liposome surface. (B) Transmitted electron image of a region shown in (A) further confirms the binding of AuC nanoparticles on the liposome. (C) Dark field transmission image of AuC nanoparticles. (D) Transmission image of AuC nanoparticles.

To further confirm the binding of AuC nanoparticles to the liposome surface, a fraction of fluorescently labeled lipid, 1,2-dimyristoyl-*sn*-glycero-3-phosphoethanolamine-*N*-lissamine rhodamine B sulfonyl (DMPE-RhB, excitation/emission = 550/590 nm), was doped into the liposome membranes. It was expected that AuC binding would quench the fluorescence dye underneath or nearby the AuC particles because of a fluorescence resonance energy transfer (FRET) mechanism. AuC nanoparticles were mixed with fluorescently labeled liposomes with a molar ratio (M_{AuC}/M_L) ranging from 0 to 280. Fluorescence emission intensity at 590 nm was recorded, and quenching yield was calculated as follows: quenching yield (%) = $(1 - I_{AuC-L}/I_L) \times 100$, in which I_{AuC-L} and I_L represent the fluorescence intensity of RhB-labeled liposomes in the presence and absence of AuC nanoparticles, respectively. As shown in Figure 4A, when the M_{AuC}/M_L molar ratio increased, the quenching yield increased and reached 100% at $M_{AuC}/M_L = 280$. Since the diameters of liposomes and AuC nanoparticles were about 88 and 4 nm respectively, the estimated surface coverage of AuC on the liposome surface was about 14% at the M_{AuC}/M_L ratio of 280:1, assuming that all AuC attached to the liposome surface. According to the FRET mechanism, the adsorbed AuC particles can effectively quench DMPE-RhB probes not only underneath the AuC but also within the 2−5 nm region surrounding the AuC particles. This will result in a near 100% theoretical quenching yield at 14% surface coverage, which is consistent with what has been observed in Figure 4A. Although more AuC particles might be able to adsorb onto the ~86% unoccupied liposome surface, further studies demonstrated that the quenching yield remained as a plateau of 100% when more AuC was added into the solution above the fully quenching point of $M_{AuC}/M_L = 280$. Figure 4A inset shows the representative fluorescence emission spectra of the AuC-liposome in the range of 500−650 nm at different M_{AuC}/M_L ratios with an excitation wavelength of 470 nm. We found that this excitation wavelength can effectively excite the DMPE-RhB probe doped in liposome membranes while minimally interfering with the fluorescence emission spectra.

Next we investigated the acid-responsive detachment of AuC from the liposomes. Hypothetically, when the environment pH value is reduced below the pK_a value of carboxylic acid, the negatively charged $Au{-}COO^-$ will be protonated to become neutral Au−COOH, which may detach from the cationic liposomes due to the elimination of electrostatic attraction. Subsequently, the detaching of AuC will induce a fluorescence recovery of the DMPE-RhB probes doped in

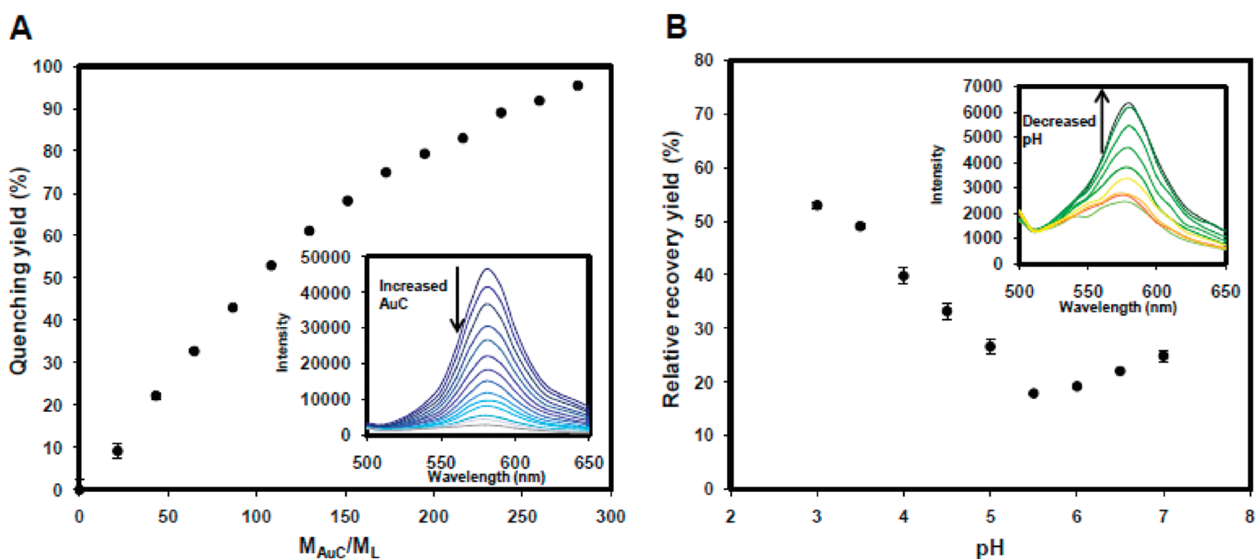

Figure 4. Fluorescence quenching and recovery yields of AuC-liposome at different AuC/liposome molar ratios (M_{AuC}/M_L) and different pH values. (A) AuC nanoparticles at different M_{AuC}/M_L molar ratios are allowed to adsorb to fluorescently labeled liposomes. Percentages of fluorescence quenching yields are plotted against M_{AuC}/M_L ratio. Inset: fluorescence emission spectra of AuC-liposome at different M_{AuC}/M_L ratios (from top to the bottom: 0, 22, 44, 66, 88, 110, 132, 154, 176, 200, 220, 240, 260, and 280). (B) Relative fluorescence recovery yield of AuC-liposome (M_{AuC}/M_L = 200) at different pH values. Inset: fluorescence emission spectra of AuC-liposome at a series of pH values (from top to the bottom: 3, 3.5, 4, 4.5, 5, 7, 6.5, 6, and 5.5).

the liposomes. To test this hypothesis, AuC-liposome solution with a M_{AuC}/M_L ratio of 200 was used to study the relative fluorescence recovery yield of DMPE-RhB at various pH values. The pH of the AuC-liposome solution was adjusted to desired values ranging from pH = 7 to 3 using buffer solutions consisting of potassium hydrogen phthalate or potassium phosphate monobasic with a final salt concentration of 5 mM. Fluorescence emission intensity at 590 nm of the AuC-liposome solutions at various pH values was recorded. Considering that the detached AuC nanoparticles suspended in the fluorescently labeled liposome solutions may quench the DMPE-RhB dyes as well through random collision, we used relative recovery yield to describe the fluorescence recovery upon pH change. The fluorescence intensity of AuC-liposome at each pH point was normalized with that of liposomes mixing with the same amount of bare gold nanoparticles (AuB), which are not modified with carboxyl group and characteristic of Au−COOH. The relative recovery yield was defined as follows: relative recovery yield (%) = $I_{AuC-L}/I_{AuB-L} \times 100$, in which I_{AuC-L} and I_{AuB-L} represent fluorescence intensity of AuC-stabilized liposomes and mixtures of liposomes and AuB at the same concentration as AuC-liposome at various pH values. As shown in Figure 4B, the relative recovery yield of DMPE-RhB-labeled AuC-liposome slightly decreased from 23% to 18% when the pH value decreased from 7 to 5.5. Then, it dramatically increased from 18 to about 55% when the pH value further decreased from 5.5 to 3. The slight decrease of the relative recovery yield from pH = 7 to 5.5 indicates that more AuC particles adsorb onto the liposomes or stronger binding between AuC and liposomes occurs at pH = 5.5 than at pH = 7. This might be because cationic lipid DOTAP becomes more positively charged at lower pH resulting in stronger charge−charge attraction between AuC and the liposomes. While when the pH value was less than 5.5 within the range of 5.5−3, the protonation effect of AuC was more dominant than any other effects, which significantly weakened the electrostatic attraction. Therefore, AuC detached from the liposome surface leading to high fluorescence recovery. Figure 4B inset shows the representative fluorescence emission spectra of the AuC-liposome in the range of 500−650 nm at different pH values ranging from 7 to 3 with an excitation wavelength of 470 nm. These fluorescence recovery results are consistent with the surface ζ potential measurements of the AuC-liposome at different pH values. We found that the surface ζ potential of the AuC-liposome increased from −25.3 ± 0.7 mV at pH = 7 to +30.1 ± 2.1 mV at pH = 4, indicating the detachment of the AuC from the liposome surface at acidic pH. The surface ζ potential of the AuC-liposome at pH = 4 is slightly higher than that of bare liposomes at pH = 7, 24.9 ± 2.3 mV (Figure 2B), which may be because the cationic lipid DOTAP is more positively charged at acidic pH.

The binding of AuC to the liposome surface at neutral pH and detaching at acidic pH were further examined by measuring UV−vis absorption of AuC-liposome at pH = 7 and 4, respectively, after the removal of unbound AuC *via* proper centrifugation. Here, HCl was used to adjust the pH of the AuC-liposome solutions instead of using buffer solutions because some UV absorption of the buffer was detected. After incubating the AuC-stabilized cationic liposomes (not fluorescently labeled) with HCl for 10 min at pH = 7 and 4, the AuC-liposome solutions were centrifuged to precipitate un-

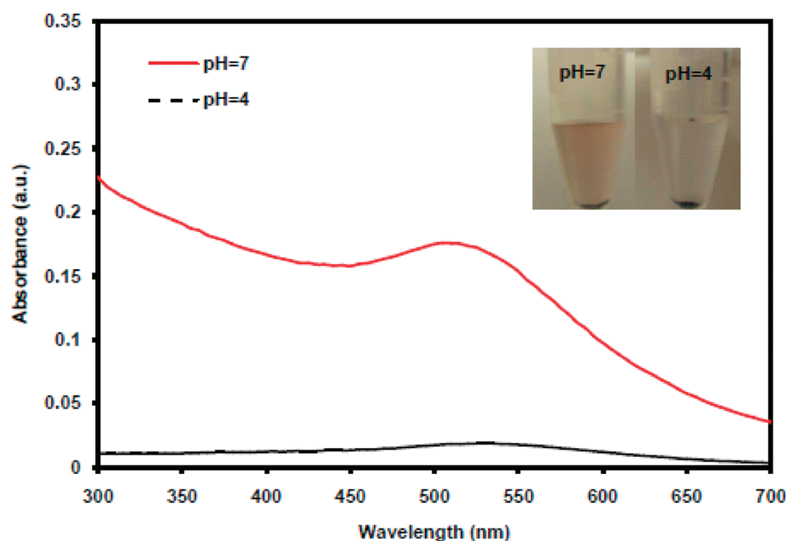

Figure 5. UV−vis absorption spectra of AuC-liposome at pH = 7 (red solid line) and pH = 4 (black dashed line) after removal of unbound AuC through centrifugation. At pH = 7, a clear UV absorption spectrum of AuC was detected, indicating the strong binding of deprotonated AuC on the liposome surface. At pH = 4, negligible UV absorption of AuC was detected, indicating the detaching of protonated AuC from the liposome surface. Inset: AuC-liposome solutions after centrifugation to remove free AuC. Red color indicates the presence of AuC in the solution at pH = 7.

bound AuC nanoparticles. The UV−vis absorption spectra of the resulted supernatants were then recorded in the range of 300 to 700 nm, as shown in Figure 5. At pH = 7, the UV absorption spectrum of AuC was clearly detected but not at pH = 4. The observed UV absorption spectra were consistent with the color difference of the supernatant, as shown in Figure 5 inset. At pH = 7, a small amount of particle precipitates was observed, while the color of the supernatant remained red, characteristic of gold nanoparticles. In contrast, at pH = 4, a large amount of particle precipitates appeared and the color of the supernatant became clear. This clear supernatant was then subjected to measuring the size and surface ζ potential using DLS with results similar as bare liposomes. These data suggest that, when the pH value (*e.g.*, pH = 7) was higher than the pK_a (~5) of carboxylic acid, AuC nanoparticles were in deprotonated form ($Au-COO^-$) and thus strongly bound to cationic liposomes. So they could not be separated from liposomes by centrifugal force. However, when the pH value (*e.g.*, pH = 4) was less than the pK_a value, AuC nanoparticles were protonated to Au−COOH form, which no longer adsorbed on the liposomes. The unbound Au−COOH particles were readily separated from the solution by centrifugation.

After having demonstrated the binding and detaching of AuC nanoparticles from cationic liposomes upon environment acidity changes, we finally examined the controllable fusion activity of the liposomes mediated by the AuC nanoparticles. To this end, we prepared anionic liposomes consisting of EggPC and lauric acid (LA), which were mixed with AuC-stabilized cationic liposomes at different pH values. It was expected that bare cationic liposomes would bind to and fuse with anionic liposomes intimately after the AuC nanoparticles were protonated and detached from the cationic liposomes. To monitor the fusion process and the fusion extent, the anionic liposomes were prelabeled with a FRET pair of chromophores, and the change in FRET signal was measured upon mixing the FRET-labeled anionic liposomes with AuC-stabilized cationic liposomes at pH = 7 and 4. FRET is a widely used technique that precisely measures the distance of two subjects at the molecular level based on an energy transfer mechanism of two chromophores.[31] When the two chromophores are in close proximity (<10 nm), the excited donor can transfer energy to the acceptor through a nonradiative long-range dipole−dipole coupling mechanism. Here we incorporated a fluorescence donor (C_6NBD, excitation/emission = 470/520 nm) and a fluorescence acceptor (DMPE-RhB, excitation/emission = 550/590 nm) into the lipid membranes of anionic liposomes. By controlling the molar ratio between the donor and the acceptor, we prepared the fluorescent anionic liposomes in which the fluorescence emission from the donor was completely quenched by the acceptor.[32] We hypothesized that, if the anionic liposomes fuse with the cationic liposomes, the spread of the donor and acceptor chromophores within the fused liposomes will alleviate or eliminate the FRET efficiency, resulting in fluorescence recovery of the donor.

For this fusion study, AuC-stabilized cationic liposomes (M_{AuC}/M_L = 200) were first adjusted to pH = 7 and 4 using buffer solutions. The resulting unbound AuC nanoparticles were removed from the solutions *via* 10 min centrifugation at 1.3×10^4 rpm in order to eliminate the fluorescence quenching effect of free AuC in the solutions through random collision. Subsequently, the cationic liposomes were mixed with the FRET-labeled anionic liposomes at a molar ratio of 7:1.

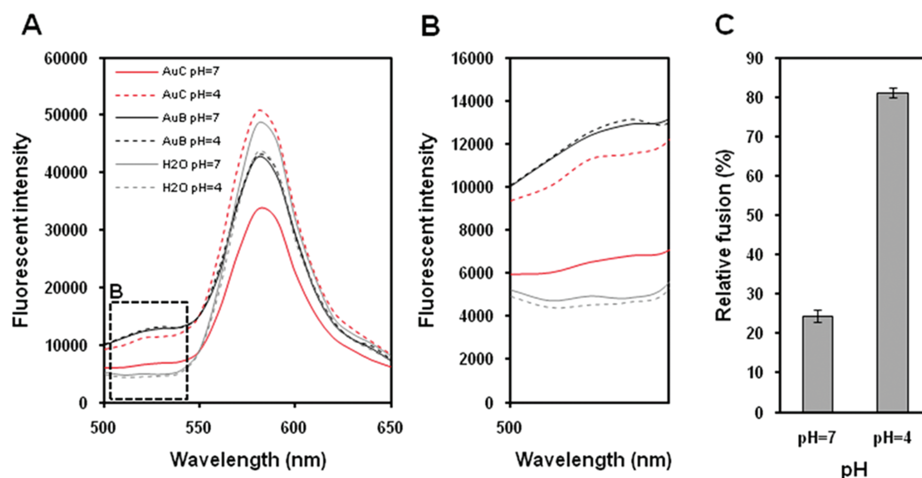

Figure 6. FRET measurement of AuC-mediated liposome fusion at pH = 7 and 4. A fluorescent donor (C_6NBD) and a fluorescent quencher (DMPE-RhB) were simultaneously incorporated into the anionic liposomes with a proper molar ratio that the quencher effectively quenched the fluorescence emission from the donor. The FRET-labeled anionic liposomes were then mixed with AuC-stabilized cationic liposomes. (A) Fluorescence emission spectra of C_6NBD and DMPE-RhB with an excitation wavelength of 470 nm. Red lines represent AuC cationic liposomes mixing with the anionic liposomes at pH = 7 (solid line) and pH = 4 (dashed line). Black lines represent AuB cationic liposomes mixing with the anionic liposomes at pH = 7 (solid line) and pH = 4 (dashed line). Gray lines represent an aqueous solution of the anionic liposomes alone without any gold nanoparticles or cationic liposomes at pH = 7 (solid line) and pH = 4 (dashed line). (B) Zoom in image of fluorescence emission spectra of C_6NBD (donor) at different conditions from panel A. (C) Relative fusion activity of AuC cationic liposomes with anionic liposomes in contrast to AuB cationic liposomes at pH = 7 and 4.

The mixtures were then excited at the wavelength of 470 nm, and fluorescence emission spectra in the range of 500−650 were recorded, as shown in Figure 4A. Since the fluorescent receptor DMPE-RhB was also excited at the 470 nm, resulting in a dominant emission peak at 590 nm, we zoomed in to the 500−540 nm emission window, which was predominantly from the C_6NBD (Figure 6B). We found that significant fluorescence recovery of C_6NBD occurred at pH = 4 as compared to at pH = 7. The most plausible explanation is that at pH = 7 Au−COO^- nanoparticles strongly bind to the cationic liposomes and prevent them from fusing with anionic liposomes. However, at pH = 4, the protonated Au−COOH nanoparticles detach from the cationic liposomes, resulting in bare cationic liposomes that can effectively fuse with the anionic liposomes. To rule out the possibility that pH adjustment will affect the FRET efficiency within the anionic liposomes, FRET-labeled anionic liposomes adjusted to the corresponding pH values and concentrations without mixing with cationic liposomes were applied as negative controls. When the control samples were excited at 470 nm, no considerable fluorescence emission difference at 530 nm was detected at pH = 7 and 4. Additionally, AuB nanoparticles (no carboxyl modification) were used as positive controls. Strong fluorescence emission of C_6NBD at 530 nm appeared at both pH = 7 and pH = 4, indicating that AuB nanoparticles do not bind tightly to the cationic liposomes to prevent them from fusing with the anionic liposomes at both neutral and acidic pH values. Figure 6C highlights the relative fusion efficiency of AuC cationic liposomes with anionic liposomes over AuB cationic liposomes with anionic liposomes, taking anionic liposomes alone at the corresponding pH values and concentrations as background. The relative fusion ability at different pH values was calculated as follows: relative fusion (%) = $(I_{530,AuC} - I_{530,H_2O})/(I_{530,AuB} - I_{530,H_2O}) \times 100$, in which $I_{530,AuC}$ represents fluorescence emission intensity at 530 nm of the AuC cationic liposomes mixing with the anionic liosomes; $I_{530,AuB}$ represents fluorescence emission intensity at 530 nm of the AuB cationic liposomes mixing with the anionic liosomes; I_{530,H_2O} represents fluorescence emission intensity at 530 nm of the anionic liposomes alone. As shown in Figure 6C, the relative fusion yield of AuC cationic liposomes was 24.4 ± 1.6 at pH = 7 and 81.1 ± 1.2 at pH = 4, indicating the feasibility of using AuC to mediate the fusion activity of liposomes.

CONCLUSIONS

In conclusion, phospholipid liposomes with acid-responsive stability and fusion activity were formed by attaching carboxyl-modified gold nanoparticles to the outer surface of cationic liposomes. At neutral pH, the negatively charged gold nanoparticles bound to the surface of cationic liposomes (diameter ~ 90 nm; surface ζ potential ~ +25 mV), resulting in a slight size increase and a dramatic surface charge change to ~ −25 mV. The adsorbed gold nanoparticles effectively quenched the fluorescent dyes doped in the liposome membranes with a quenching yield up to 100%. In contrast at acidic pH values (*e.g.*, pH < 5), the gold nanoparticles

detached from the liposome membranes at an extent depending on the environment acidity, resulting in fluorescence recovery of the dyes. The binding and detaching of gold nanoparticles from the liposomes were further confirmed by UV−vis absorbance measurements. It was also demonstrated that the adsorption of gold nanoparticles can freeze the liposomes from fusing against one another, while the fusion activity of liposomes resumes at acidic environments due to the detaching of gold particle stabilizers. We speculate that similar strategy can be generalized to anionic liposomes using amine-modified gold nanoparticles, which will be stable at neutral condition but destabilized at basic environments in which the amine will be deprotonated. Since the stability issues of liposomes have imposed negative impacts on their medical and biological applications as a drug delivery vehicle or functional nanocontainer, this work may provide a new paradigm of using liposomes as an environment-responsive nanocarrier with controllable stability and fusion activity.

EXPERIMENTAL SECTION

Materials. Hydrogenated L-α-phosphatidylcholine (EggPC), 1,2-di-(9*Z*-octadecenoyl)-3-trimethylammonium propane (DOTAP), Phytosphing, and 1,2-dimyristoyl-*sn*-glycero-3-phosphoethanolamine-*N*-lissamine rhodamine B sulfonyl (DMPE-RhB), and C_6-NBD were purchased from Avanti Polar Lipids, Inc. Lauric acic (LA) was obtained from Sigma Aldrich (St Louis, MO). In order to prepare carboxyl-functionalized gold nanoparticles (AuC), the following chemicals were purchased: hydrogen tetrachloroaurate ($HAuCl_4$) (ACROS Organics), sodium borohydride ($NaBH_4$) (ACROS Organics), and 3-mercaptopropionic acid (MPA) (Sigma Aldrich). Potassium hydrogen phthalate and potassium phosphate monobasic were purchased from EMD and Sigma Aldrich, respectively, in order to prepare buffer solutions.

Preparation of Carboxyl-Modified Gold Nanoparticles (AuC). AuC nanoparticles were prepared by a sodium borohydride reduction method described in full detail elsewhere.[29,30] Briefly, aqueous solution of $HAuCl_4$ (10^{-4} M, 50 mL) was reduced by 0.005 g of $NaBH_4$ at ice cold temperature, resulting in the formation of bare gold nanoparticles (AuB). AuB nanoparticles were functionalized with carboxyl groups by overnight incubation with MPA (4×10^{-4} M). The resulting AuC nanoparticles were washed three times by an Amicon Ultra-4 centrifugal filter with a molecular weight cutoff of 10 kDa (Millipore, Billerica, MA) and suspended in aqueous solution at pH = 6.8.

Preparation and Characterization of Liposomes and AuC-Liposome. Cationic liposomes consisting of EggPC (zwitterionic phospholipid) and DOTAP (cationic phospholipid) were prepared through the well-known extrusion method.[28] Briefly, 1.5 mg of EggPC and DOTAP mixture (weight ratio = 9:1) were dissolved in 1 mL of chloroform. The solvent was evaporated by blowing argon gas over it for 15 min. Then, the dried lipid films were hydrated with 3 mL of deionized water, followed by vortexing for 1 min and sonicating for 3 min in a bath sonicator (Fisher Scientific FS30D) to produce multilamellar vesicles (MLVs). A Ti probe (Branson 450 sonifier) was used to sonicate the MLVs for 1−2 min at 20 W to produce unilamellar vesicles. To form narrowly distributed small unilamellar vesicels (SUVs), the solution was extruded through a 100 nm pore-sized polycarbonate membrane 11 times. AuC-stabilized liposomes (AuC-liposome) were prepared by mixing liposomes and AuC nanoparticles at desired molar ratios under gentle bath sonication for 10 min.

The hydrodynamic size and surface ζ potential of the prepared liposomes and AuC-liposome were assessed by using the Malvern Zetasizer ZS (Malvern Instruments, UK). The mean diameter and ζ potential were determined through dynamic light scattering (DLS) and electrophoretic mobility measurements, respectively. All characterization measurements were repeated three times at 25 °C. The morphology and structure of the AuC-liposome were characterized by a Hitachi HD2000 scanning transmission electron microscope (STEM) equipped with a cold cathode field emission electron source and a turbo-pumped main chamber. Samples for STEM characterization were prepared by dispersing a solution containing the AuC-liposome onto the surface of a carbon film coated Cu grid. The samples were air-dried and then coated with a thin amorphous carbon film by evaporation. All images were recorded in the STEM as scanned beam images, using the secondary electron signal, which provides surface topology detail, the direct transmitted electron beam (unscattered electrons) or the diffracted transmission electrons collected on an annular dark field detector.

Fluorescence Quenching and Recovery Studies. DMPE-RhB-labeled liposomes were prepared by mixing 0.5 mol % of DMPE-RhB with EggPC and DOTAP prior to liposome preparation. To monitor the quenching effect of AuC on the fluorescently labeled liposomes, AuC nanoparticles were mixed with the liposomes at desired molar ratios (M_{AuC}/M_L) ranging from 0 to 280, followed by 10 min sonication. The fluorescence emission spectra of DMPE-RhB in the range of 500−650 nm were measured by using a fluorescent spectrophotometer (Infinite M200, TECAN, Switzerland) at an excitation wavelength of 470 nm. The emission peak at 590 nm was selected to quantify the fluorescence quenching yield.

To study the fluorescence recovery yield of DMPE-RhB-labeled AuC-liposome at different pH values, the AuC-liposome solution with a $M_{AuC}/M_L = 200$ was selected. The DMPE-RhB-labeled AuC-liposome were adjusted to desired pH values using proper buffer solutions with target pH values (potassium hydrogen phthalate buffer for pH = 3−5, and potassium phosphate monobasic buffer for pH = 5.5−7). The actual pH value of each AuC-liposome solution was measured by an Orion 3-star plus portable pH meter. The salt concentration of each AuC-liposome solution after pH adjustment was 5 mM. The fluorescence emission spectra of DMPE-RhB were measured as previously described. The mixtures of fluorescently labeled liposome and bare gold nanoparticles (AuB, no carboxyl modification) at the same molar ratios were used as positive controls.

The UV−Vis Absorption Spectra of AuC-Liposomes at pH = 7 and 4. AuC-liposome were prepared following the protocol described above. To adjust the pH value of the AuC-liposome solution to pH = 4, 0.1 M HCl was used because it did not induce any undesirable UV absorption background. Unbound AuC nanoparticles were removed from the solution by centrifugation at 1.3×10^4 rpm for 10 min. Absorption spectra in the range of 300−700 nm were recorded by a spectrophotometer. To exclude possible UV absorption from the cationic liposomes and background, free liposomes (without AuC addition) at the same concentration and pH value as the AuC-liposome were measured, whose signal was subtracted from the measured AuC-liposome UV absorption spectra. All measurements were repeated three times.

AuC-Liposome Fusion Studies. To investigate the fusion activity of AuC-liposome against other liposomes or target cells at different pH values, negatively charged liposomes consisting of EggPC and lauric acid (weight ratio = 9:1) were synthesized by an extrusion method as described above to mimic negatively charged cells. These anionic liposomes were labeled with a fluorescence resonance energy transfer (FRET) pair of chromophores, a fluorescent donor (C_6NBD, 0.1 mol %), and a fluorescent quencher (DMPE-RhB, 0.5 mol %). AuC cationic liposome ($M_{AuC}/M_L = 200$) solutions were prepared and adjusted to pH = 7 and 4. Unbound AuC nanoparticles were removed by centrifugation at 1.3×10^4 rpm for 10 min. The supernatants of the AuC cationic liposomes were mixed with FRET-labeled anionic liposomes with a molar ratio of 7:1. Consequently, fluorescence emission spectra at the

range of 500−650 nm were obtained by exciting the samples at 470 nm using a fluorescent spectrophotometer. AuB cationic liposome mixtures at the corresponding molar ratios and pH values were used as positive controls. The FRET-labeled anionic liposomes alone (without the addition of cationic liposomes) at the corresponding concentrations and pH values were used as negative controls. All measurements were carried out at 25 °C and repeated three times.

Acknowledgment. This work is supported by National Institutes of Health Grant U54CA119335 and the University of California San Diego.

REFERENCES AND NOTES

1. Torchilin, V. P. Recent Advances with Liposomes as Pharmaceutical Carriers. *Nat. Rev. Drug Discovery* **2005**, *4*, 145–160.
2. Lian, T.; Ho, R. J. Y. Trends and Developments in Liposome Drug Delivery Systems. *J. Pharm. Sci.* **2001**, *90*, 667–680.
3. Zhang, L.; Gu, F. X.; Chan, J. M.; Wang, A. Z.; Langer, R. S.; Farokhzad, O. C. Nanoparticles in Medicine: Therapeutic Applications and Developments. *Clin. Pharmacol. Ther.* **2008**, *83*, 761–769.
4. Barenholz, Y. Liposome Application: Problems and Prospects. *Curr. Opin. Colloid Interface Sci.* **2001**, *6*, 66–77.
5. Haluska, C. K.; Riske, K. A.; Marchi-Artzner, V.; Lehn, J.-M.; Lipowsky, R.; Dimova, R. Time Scales of Membrane Fusion Revealed by Direct Imaging of Vesicle Fusion with High Temporal Resolution. *Proc. Natl. Acad. Sci. U.S.A.* **2006**, *103*, 15841–15846.
6. Lei, G.; MacDonald, R. C. Lipid Bilayer Vesicle Fusion: Intermediates Captured by High-Speed Microfluorescence Spectroscopy. *Biophys. J.* **2003**, *85*, 1585–1599.
7. Marrink, S.; Mark, A. E. The Mechanism of Vesicle Fusion as Revealed by Molecular Dynamics Simulations. *J. Am. Chem. Soc.* **2003**, *125*, 11144–11145.
8. Zhang, L.; Granick, S. How to Stabilize Phospholipid Liposome (Using Nanoparticles). *Nano Lett.* **2006**, *6*, 694–698.
9. Prausnitz, M. R.; Langer, R. Transdermal Drug Delivery. *Nat. Biotechnol.* **2008**, *26*, 1261–1268.
10. Sinico, C.; Fadda, A. M. Vesicular Carriers for Dermal Drug Delivery. *Expert Opin. Drug Delivery* **2009**, *6*, 813–825.
11. Kostarelos, K.; Tadros, T. F.; Luckham, P. F. Physical Conjugation of (Tri-) Block Copolymers to Liposomes toward the Construction of Sterically Stabilized Vesicle Systems. *Langmuir* **1999**, *15*, 369–376.
12. Ringsdorf, H.; Schlarb, B.; Venzmer, J. Molecular Architecture and Function of Polymeric Oriented Systems—Models for the Study of Organization, Surface Recognition, and Dynamics of Biomembranes. *Angew. Chem., Int. Ed. Engl.* **1988**, *27*, 113–158.
13. Semple, S. C.; Chonn, A.; Cullis, P. R. Influence of Cholesterol on the Association of Plasma Proteins with Liposomes. *Biochemistry* **1996**, *35*, 2521–2525.
14. Corma, A.; Díaz, U.; Arrica, M.; Fernández, E.; Ortega, Í. Organic−Inorganic Nanospheres with Responsive Molecular Gates for Drug Storage and Release. *Angew. Chem., Int. Ed.* **2009**, *48*, 6247–6250.
15. Moghimi, S. M.; Szebeni, J. Stealth Liposomes and Long Circulating Nanoparticles: Critical Issues in Pharmacokinetics, Opsonization and Protein-Binding Properties. *Prog. Lipid Res.* **2003**, *42*, 463–478.
16. Woodle, M. C. Controlling Liposome Blood Clearance by Surface-Grafted Polymers. *Adv. Drug Delivery Rev.* **1998**, *32*, 139–152.
17. Davis, M. E.; Chen, Z. G.; Shin, D. M. Nanoparticle Therapeutics: An Emerging Treatment Modality for Cancer. *Nat. Rev. Drug Discovery.* **2008**, *7*, 771–782.
18. Castro, G. A.; Ferreira, L. A. Novel Vesicular and Particulate Drug Delivery Systems for Topical Treatment of Acne. *Expert Opin. Drug Delivery* **2008**, *5*, 665–679.
19. Schafer-Korting, M.; Mehnert, W.; Korting, H. C. Lipid Nanoparticles for Improved Topical Application of Drugs for Skin Diseases. *Adv. Drug Delivery Rev.* **2007**, *59*, 427–443.
20. Schmid-Wendtner, M. H.; Korting, H. C. The pH of the Skin Surface and Its Impact on the Barrier Function. *Skin Pharmacol. Physiol.* **2006**, *19*, 296–302.
21. Greenman, J. Follicular pH and the Development of Acne. *Int. J. Dermatol.* **1981**, *20*, 656–658.
22. Holland, D. B.; Cunliffe, W. J. Skin Surface and Open Comedone pH in Acne Patients. *Acta Derm. Venereol.* **1983**, *63*, 155–158.
23. Wang, B.; Zhang, L.; Bae, S. C.; Granick, S. Nanoparticle-Induced Surface Reconstruction of Phospholipid Membranes. *Proc. Natl. Acad. Sci. U.S.A.* **2008**, *105*, 18171–18175.
24. Zhang, L.; Hong, L.; Yu, Y.; Bae, S. C.; Granick, S. Nanoparticle-Assisted Surface Immobilization of Phospholipid Liposomes. *J. Am. Chem. Soc.* **2006**, *128*, 9026–9027.
25. Liptak, M. D.; Shields, G. C. Accurate pK(a) Calculations for Carboxylic Acids Using Complete Basis Set and Gaussian Models Combined with CPCM Continuum Solvation Methods. *J. Am. Chem. Soc.* **2001**, *123*, 7314–7319.
26. Shukla, R.; Bansal, V.; Chaudhary, M.; Basu, A.; Bhonde, R. R.; Sastry, M. Biocompatibility of Gold Nanoparticles and Their Endocytotic Fate Inside the Cellular Compartment: A Microscopic Overview. *Langmuir* **2005**, *21*, 10644–10654.
27. Boisselier, E.; Astruc, D. Gold Nanoparticles in Nanomedicine: Preparations, Imaging, Diagnostics, Therapies and Toxicity. *Chem. Soc. Rev.* **2009**, *38*, 1759–1782.
28. Mayer, L. D.; Hope, M. J.; Cullis, P. R. Vesicles of Variable Sizes Produced by a Rapid Extrusion Procedure. *Biochim. Biophys. Acta* **1986**, *858*, 161–168.
29. Aryal, S.; Remant, B. K. C.; Dharmaraj, N.; Bhattarai, N.; Kim, C. H.; Kim, H. Y. Spectroscopic Identification of S−Au Interaction in Cysteine Capped Gold Nanoparticles. *Spectrochim. Acta A* **2006**, *63*, 160–163.
30. Patil, V.; Malvankar, R. B.; Sastry, M. Role of Particle Size in Individual and Competitive Diffusion of Carboxylic Acid Derivatized Colloidal Gold Particles in Thermally Evaporated Fatty Amine Films. *Langmuir* **1999**, *15*, 8197–8206.
31. Ha, T. Single-Molecule Fluorescence Resonance Energy Transfer. *Methods* **2001**, *25*, 78–86.
32. Yang, D.; Pornpattananangkul, D.; Nakatsuji, T.; Chan, M.; Carson, D.; Huang, C. M.; Zhang, L. The Antimicrobial Activity of Liposomal Lauric Acids against *Propionibacterium acnes*. *Biomaterials* **2009**, *30*, 6035–6040.